Chemical Geology 654 (2024) 122065

Contents lists available at ScienceDirect

Chemical Geology

journal homepage: www.elsevier.com/locate/chemgeo

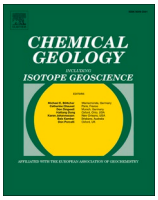

Heavy halogen impact on Raman water bands at high pressure: Implications for salinity estimations in fluid inclusions

Tobias Grützner [a,b,c,*], Hélène Bureau [a]

[a] Institut de Minéralogie, de Physique des Matériaux et de Cosmochimie (IMPMC), Sorbonne Université Paris, CNRS UMR 7590, MNHN, IRD UR 206, 4 place Jussieu, 75252 Paris Cedex 05, France
[b] Research School of Earth Sciences, Australian National University, Canberra, Australia
[c] Institut für Geowissenschaften, Goethe-Universität Frankfurt, Germany

ARTICLE INFO

Editor: Claudia Romano

Original content: Raman Water bands on experimental sodium-halogen solutions at various pressure and concentration (Original data)

Keywords:
Raman
Water bands
Fluid inclusion
Halogens
Salinity
High pressure

ABSTRACT

We present a new experimental dataset on the impact of the heavy halogens chlorine, bromine and iodine on the Raman water bands concerning pressure and their concentration at room temperature. These experiments were conducted at ambient temperature, with variations in halogen concentration and pressure ranging from 0 to 1.4 GPa.

The strength of the Raman water band shift change increases with the ionic size from chlorine, over bromine, to iodine. Our experiments further demonstrate that increased pressure diminishes the impact of the halogen shift change to a varying extent for each of the three halogens. This finding can have significant implications for the salinity calculation of fluid inclusions in minerals such as quartz or olivine. Particularly in the low salinity range, the concentration can be markedly underestimated if the pressure effect is neglected. For experiments in diamond anvil cells involving halogens dissolved in water, the change in Raman water band shifts can serve either as a new tool to monitor pressure, or to monitor the salinity.

1. Introduction

Halogens play a pivotal role as volatile elements, significantly impacting geodynamic processes. They constitute essential components of volcanic fumaroles and volcanic ejecta. Upon release into the atmosphere, halogens contribute to ozone destruction. In crustal hydrothermal fluids, halogen complexes (e.g., in saline fluids, brines, or molten salts) serve as major agents for metal transport in ore-forming processes related to hydrothermal systems (e.g., Aiuppa et al., 2009). Samples of such fluids can be found entrapped as inclusions in minerals like quartz (e.g., Brooks et al., 2019; Pankrushina et al., 2020) or olivine (e.g., Kawamoto et al., 2013) in magmatic and metamorphic rocks. Raman spectroscopy has been employed for decades to determine the salinity of fluid inclusions, especially those too small for other common techniques like microthermometry – a method that determines salinity by observing and measuring the freezing temperature of the fluid (cf. e.g., Kawamoto et al., 2013; Moncada and Bodnar, 2012; Brooks et al., 2019).

The Raman spectra of water and aqueous fluids exhibit several peaks closely grouped at 2800–3800 cm^{-1}, resulting in water stretching bands (e.g., Ratcliffe and Irish, 1982; Sun, 2009; Walrafen et al., 1986). In salty solutions or brines, halogen ions interact with the bonds of water molecules. Although ions and ionic bonding cannot be directly detected with Raman spectroscopy, their impact on the network of covalent water bonding is detectable. This effect has been the subject of numerous studies, with a substantial focus on chlorine (e.g., Dubessy et al., 2002; Đuričković et al., 2010; Georgiev et al., 1984; Mernagh and Wilde, 1989; Pankrushina et al., 2020; Sun, 2012; Sun et al., 2010; Terpstra et al., 1990) and, to a lesser extent, on the heavy halogen bromine (e.g., Terpstra et al., 1990). Halogen anions widen the water bonding network, forcing the network to change its bonding structure by favoring a certain type of bonding over others. A shift in water bands can be observed, correlating with the number of dissolved halogens and facilitating the determination of salt concentration in the solution or in mineral fluid inclusions (e.g., Dubessy et al., 2002; Đuričković et al., 2010; Georgiev et al., 1984; Mernagh and Wilde, 1989; Pankrushina et al., 2020; Sun, 2012; Sun et al., 2010; Terpstra et al., 1990).

* Corresponding author at: Research School of Earth Sciences, Australian National University, Canberra, Australia.
E-mail addresses: tobias.gruetzner@outlook.com (T. Grützner), helene.bureau@sorbonne-universite.fr (H. Bureau).

https://doi.org/10.1016/j.chemgeo.2024.122065
Received 14 December 2023; Received in revised form 14 March 2024; Accepted 24 March 2024
Available online 26 March 2024

The heavy halogens bromine and iodine possess a larger ionic size than chlorine. Their anions stretch the water network as much or even more than chlorine, causing a more pronounced alteration of the Raman shift (Terpstra et al., 1990). The impact of the cations (e.g., calcium, magnesium, sodium, potassium) in a salty solution seem to be negligible (Sun et al., 2010).

Two other factors can alter the shape of Raman water bands: (1) temperature (e.g., Krishnamurthy et al., 1983; Ratcliffe and Irish, 1982) and (2) pressure (Romanenko et al., 2018). Increasing temperature has a similar effect to increasing halogen concentrations, enhancing the resulting peak at around 3430 cm^{-1}. Pressure shifts the bands in the opposing direction: It decreases the peak at 3430 cm^{-1} and increases the peak at 3240 cm^{-1}.

While fluid inclusions in minerals are typically studied at ambient temperature and its effect can be ignored, the pressure in mineral fluid inclusions, such as those in quartz, is likely to be elevated, potentially impacting the Raman spectrum. In this study, we present a novel experimental dataset examining the impact of all three heavy halogens — chlorine, bromine, and iodine — on Raman water bands concerning pressure and halogen concentration at room temperature. We further compare our results to some natural fluid inclusion samples from other studies to demonstrate and constrain the impact of our dataset on natural fluid inclusions.

2. Experimental setup and methods

Various concentrations of NaCl, NaBr, or NaI salts were dissolved in water to synthesize salty solutions as starting materials (Table 1). Sodium-halogen salts exhibit excellent solubility in water, and sodium serves as the dominant cation in seawater-related fluids. Despite the seemingly negligible impact of cations (Sun et al., 2010), sodium was selected as the cation for all three halogens to mitigate cation effects and focus on the influence of the three halogen anions.

The experiments were conducted using a Chervin-type hydrothermal diamond anvil cell (HDAC) with a pressure-driving membrane (Chervin et al., 2001). The HDAC was equipped with 2 mm thick diamonds and culets of 1 mm diameter. The sample chamber, compressed between two diamonds, had a diameter of 500 μm, drilled as a hole into a Re gasket with an initial thickness of 200 μm. Before each experiment, the sample chamber was cleaned with ethanol, dried, and loaded with a salty solution along with a small number of ruby spheres for pressure calibration. Following HDAC closure, the membrane was connected to an inflator with a N_2 gas bottle. The membrane was initially loaded with approximately 10 to 15 bar of gas pressure, sufficient to seal the HDAC but insufficient to observe a fluorescence shift with the ruby spheres.

Table 1
Salt concentration in the starting solutions and maximum solubility values.

	NaCl				max(NaCl)[a]
g/l	10	20	50	100	*317*
mol/l	0.17	0.34	0.86	1.71	*5.42*
wt%	0.99	1.96	4.76	9.09	*24.07*

	NaBr				max(NaBr)[a]
g/l	20	50	100	150	*905*
mol/l	0.19	0.49	0.97	1.46	*8.80*
wt%	1.96	4.76	9.09	13.04	*47.51*

	NaI			max(NaI)[a]
g/l	30	100	250	*1793*
mol/l	0.20	0.67	1.67	*11.96*
wt%	2.91	9.09	20.00	*64.20*

[a] Maximum solubility in H_2O at 20 °C and ambient pressure.

Ruby fluorescence serves as a widely used pressure monitor for various DAC experiments (e.g., Chervin et al., 2001; Shen et al., 2020). The ruby shift was calibrated with the Raman to ambient pressure and had to be recalibrated for each new sample. After the ruby calibration, the water bands were measured with the Raman at ambient pressure. The pressure was then increased stepwise with an inflator, and pressure increases were monitored on the ruby fluorescence. Pressure steps were approximately 0.2 to 0.3 GPa. Depending on the salt concentration, the solution transforms into ice IV between 1.1 and 1.4 GPa (see below). After each pressure increase, the cell equilibrated the pressure for about 10 min before Raman analysis.

Raman measurements were performed with a 514.5 nm Argon laser and a Jobin-Yvon Horiba HR460 spectrometer. A constant grating of 1500 lines/mm, a slit size of 50 μm, and a 50× objective placed in front of the diamond anvil cell were used. The setup was calibrated with a 521 cm^{-1} silicon wafer, and the laser energy was controlled to remain constant at 10 mW between each measurement during the pressure equilibration period. Diamond has no effect on the Raman water bands and is widely used for these types of studies. Test runs for pure water in the DAC and in a glass cylinder showed no difference in the spectra. Measurements in the solution were conducted in the center of the sample chamber by defocusing the laser spot between both surfaces of the two diamonds (Fig. 1). Measurements in the solution were set for 10 to 30 s with 3 to 5 iterations. Measurements on the ruby spheres were conducted "live" with a repetition rate of 1 s.

It is important to note that halogens like iodine can also induce a Raman peak at around 1650 cm^{-1} (Besemer et al., 2016). However, this peak overlaps with the (extremely large) carbon peak from the diamond anvils and cannot be used for hydrothermal DAC experiments or for pressure calibration with the HDAC.

The acquisition and processing of the Raman spectra were carried out using the Labspec software. For baseline correction, peak deconvolution, and spectra smoothing (using "adjacent averaging" with a step size of 40), the Origin software was employed. Values for R_D and S_D (both are ratios that can be used to quantify the peak change numerically; see also further below) were calculated prior to spectra smoothing.

3. Results

At ambient pressure and temperature, the configuration of the water stretching bands undergoes changes based on the halogen concentration:

1. The 3428 cm^{-1} peak increases with rising halogen concentration: from 6660 counts for pure water to 7900 counts for 1.71 mol/l chlorine, 8800 counts for 1.46 mol/l bromine, and 9300 counts for 1.67 mol/l iodine, respectively.
2. The 3428 cm^{-1} peak shifts to higher wavenumbers with specific positions at 3441 cm^{-1} for chlorine, 3450 cm^{-1} for bromine, and 3460 cm^{-1} for iodine at their respective highest concentrations.
3. The minor peak at 3240 cm^{-1} becomes relatively smaller as halogen concentration increases, decreasing from 5060 counts for water to 4400 counts for chlorine, 4190 counts for bromine, and 4430 counts for iodine (Fig. 2).

At a constant halogen concentration, the characteristics of the water stretching bands evolve with increasing pressure:

1. The 3428 cm^{-1} peak decreases with rising pressure: from 6975 counts at 0 GPa to 5960 counts at 1.1 GPa for 0.34 mol/l chlorine, from 8800 counts at 0 GPa to 7350 counts at 1.1 GPa for 1.45 mol/l bromine, and from 6315 counts at 0 GPa to 6010 counts at 1.39 GPa for 0.2 mol/l iodine.
2. The 3428 cm^{-1} peak shifts to lower wavenumbers, with new positions at 3390 cm^{-1} for chlorine, from 3450 to 3435 cm^{-1} for

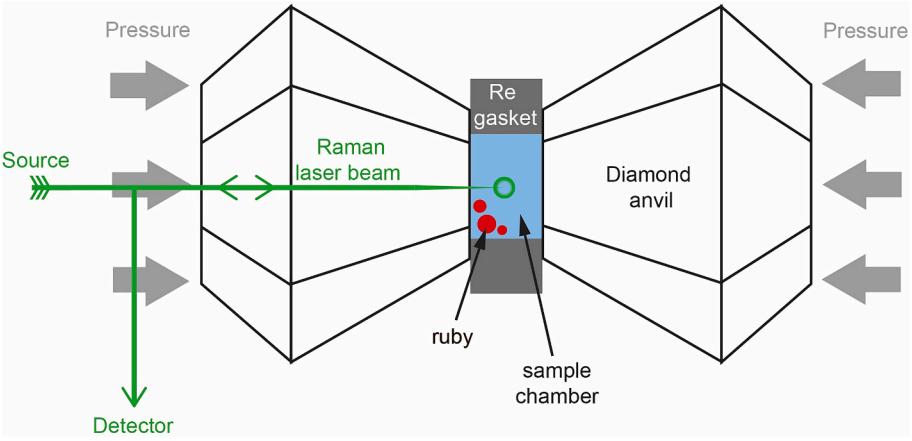

Fig. 1. Experimental Setup: The saline solution was loaded into a hydrothermal diamond anvil cell (HDAC). Pressure control was achieved using an external inflator, and pressure levels were monitored via the fluorescence of ruby spheres suspended in the sample chamber. Raman measurements in the solution were performed at the center of the sample chamber by intentionally defocusing the laser spot between the surfaces of the two diamonds.

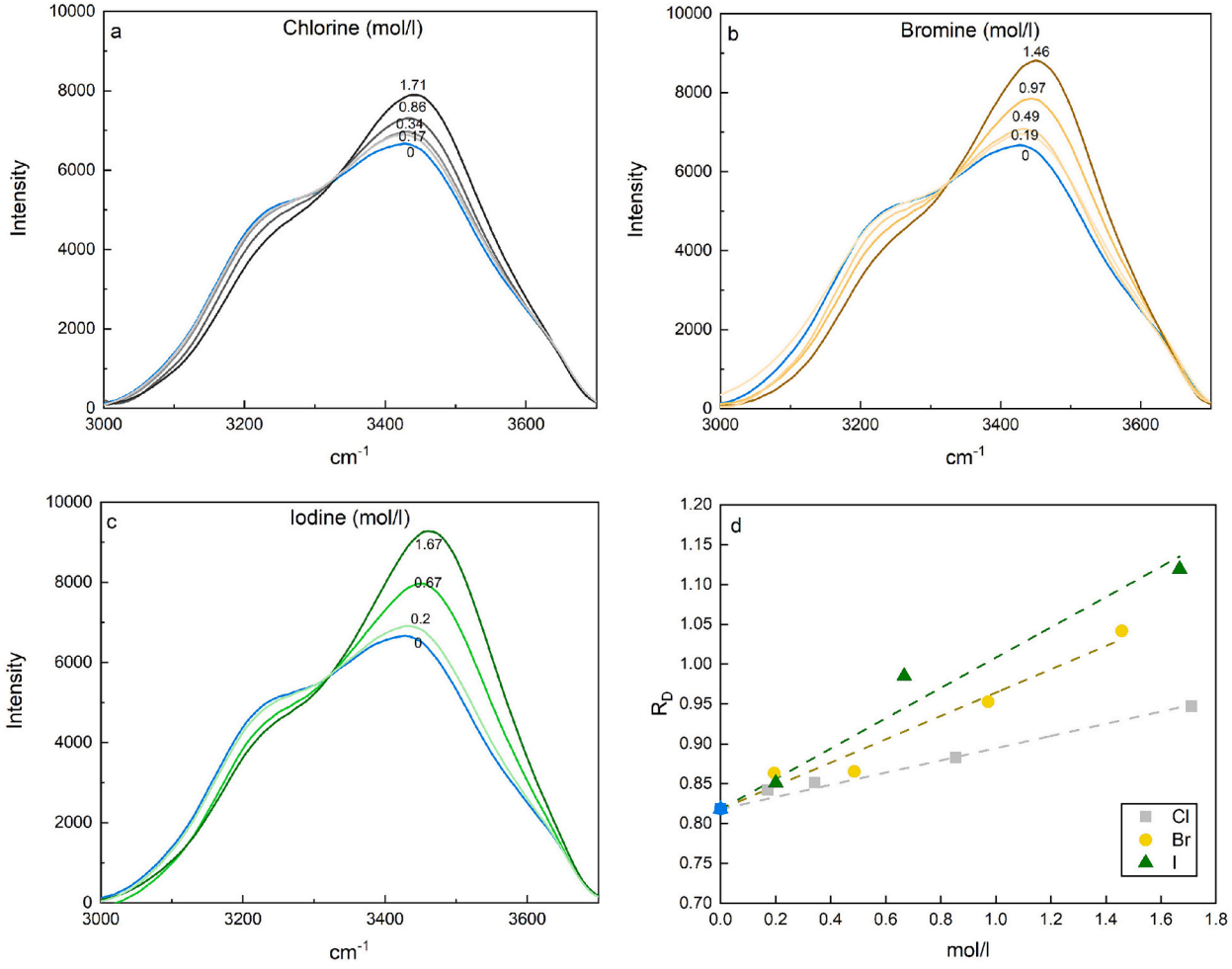

Fig. 2. The Raman water bands of saline solutions with varying concentrations of a) chlorine, b) bromine, and c) iodine are depicted. The halogen concentrations are indicated on the spectrum in mol/l. Notably, the resulting peak of the water bands at 3428 cm^{-1} exhibits an increase and shifts further to the right with escalating halogen concentration. The Raman spectrum of pure water is represented in blue. In d), there is a discernible increase in R_D with escalating concentrations of chlorine, bromine, and iodine. This increase is characterized by a larger sum of slopes between 3325 cm^{-1} and 3600 cm^{-1}, and a heightened peak at 3428 cm^{-1}. The observed effects are smallest for chlorine and most pronounced for iodine. (For interpretation of the references to colour in this figure legend, the reader is referred to the web version of this article.)

bromine, and from 3430 to 3390 cm^{-1} for iodine at their respective highest pressures.

3. The minor peak at 3240 cm^{-1} becomes relatively larger with increasing pressure, exhibiting a slight increase from 4970 to 5140 counts for chlorine, from 4190 to 4590 counts for bromine, and from 4960 to 5255 counts for iodine (Fig. 3).

4. Discussion

4.1. Halogen concentration and ionic size

The correlation between the change in the water bands' peak and varying halogen concentration, in addition to ionic size, aligns well with findings from previous studies (Dubessy et al., 2002; Đuričković et al., 2010; Georgiev et al., 1984; Mernagh and Wilde, 1989; Pankrushina et al., 2020; Sun et al., 2010; Terpstra et al., 1990). The observed shift change strength correlates directly with the ionic size of the halogens: Chlorine exhibits the smallest shift, iodine the largest, and bromine falls in between for comparable concentrations (cf. Terpstra et al., 1990 for chlorine and bromine).

Since ionic bonds are not Raman active, NaCl, NaBr, and NaI do not have observable modes of their own, neither as salts nor as dissolved ions in water (Bakker, 2004; Ni et al., 2006; Terpstra et al., 1990). Raman spectroscopy enables the observation of the vibration of covalent bonds, which, in this study, is the chemical vibration of water. The halogen anions are indirectly observed as they modify the vibrations of water bonding. The evolving shape of the Raman spectra in Fig. 2 illustrates that different halogens influence the dominant bonding type in the water structure, leading to a reduction in hydrogen bonding in water. Fig. 4 presents a deconvolution of the water stretching band into three major Gaussian components representing different bonding types for water molecules:

Peak 1 of the first Gaussian component at 3327 cm^{-1} is attributed to 4 hydrogen bonds per water molecule, involving two electron donors and two acceptors (DDAA). This peak diminishes with increasing halogen content. Peak 2 at 3431 cm^{-1} is attributed to 2 hydrogen bonds (DA) and becomes the predominant bonding type with increasing halogen content. Peak 3 at 3565 cm^{-1} is attributed to 3 hydrogen bonds per water molecule (DDA). It plays a minor role in pure water as well as in salty solutions (e.g., Sun, 2009). With the addition of salt, the increasing presence of cations and anions breaks the hydrogen bonds in the water network, forming ionic bonds.

The deconvolution of the Raman water bands confirms the reduction of hydrogen bonding in water with the addition of various halogens, as well as with their increasing ionic size.

4.2. R_D as numerical value for the changing effect

To quantify the changing shift of the water stretching bands, Đuričković et al. (2010) introduced the ratio S_D, defined by the formula:

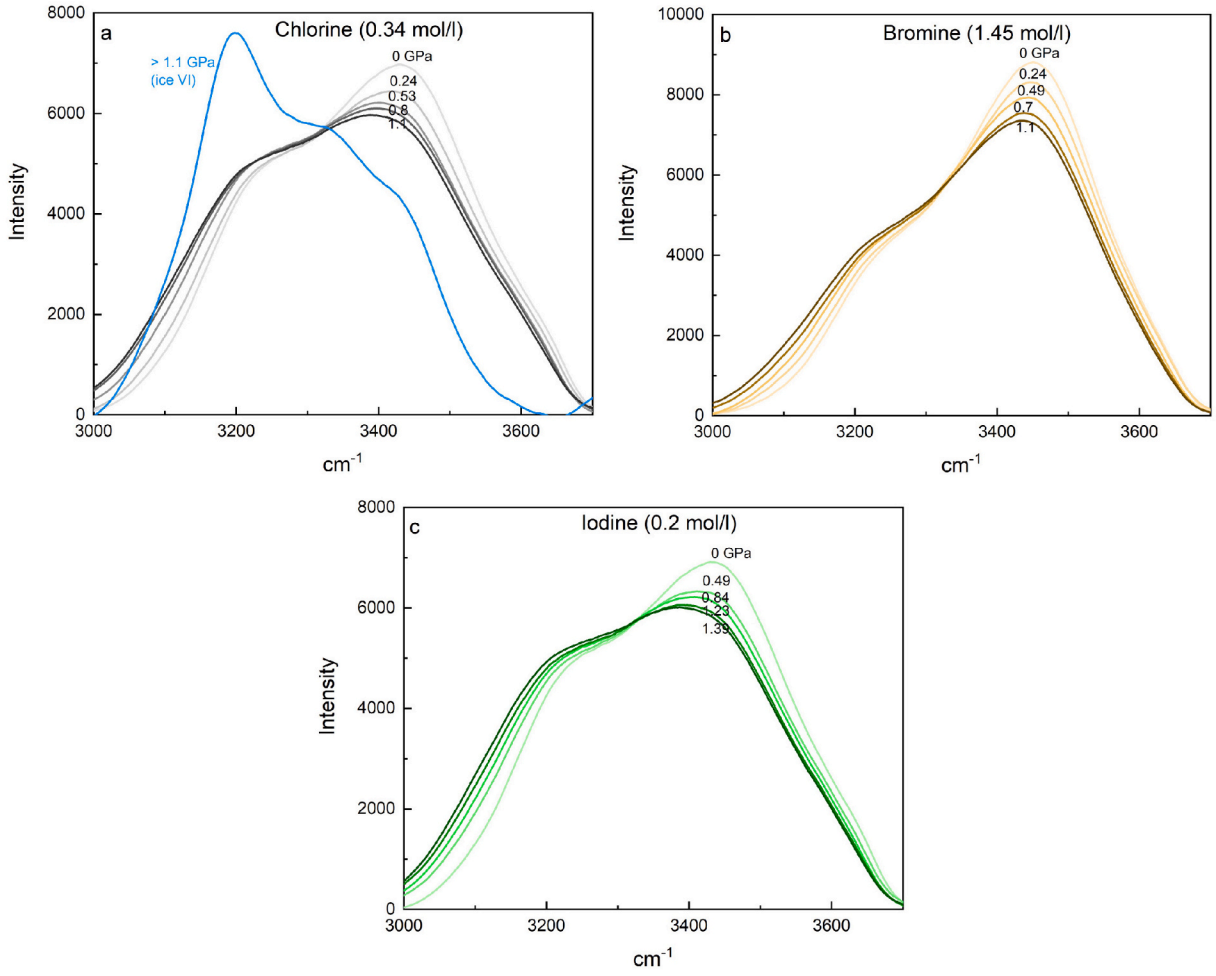

Fig. 3. The Raman water bands of saline solutions are presented with fixed halogen concentrations and varying pressure: a) 0.34 mol/l chlorine, b) 1.45 mol/l bromine, and c) 0.2 mol/l iodine. The pressure is indicated in GPa on the spectra. Notably, the resulting peaks exhibit a reduction in intensity with increasing pressure and shift towards lower wavenumbers, indicating a leftward shift in the spectra.

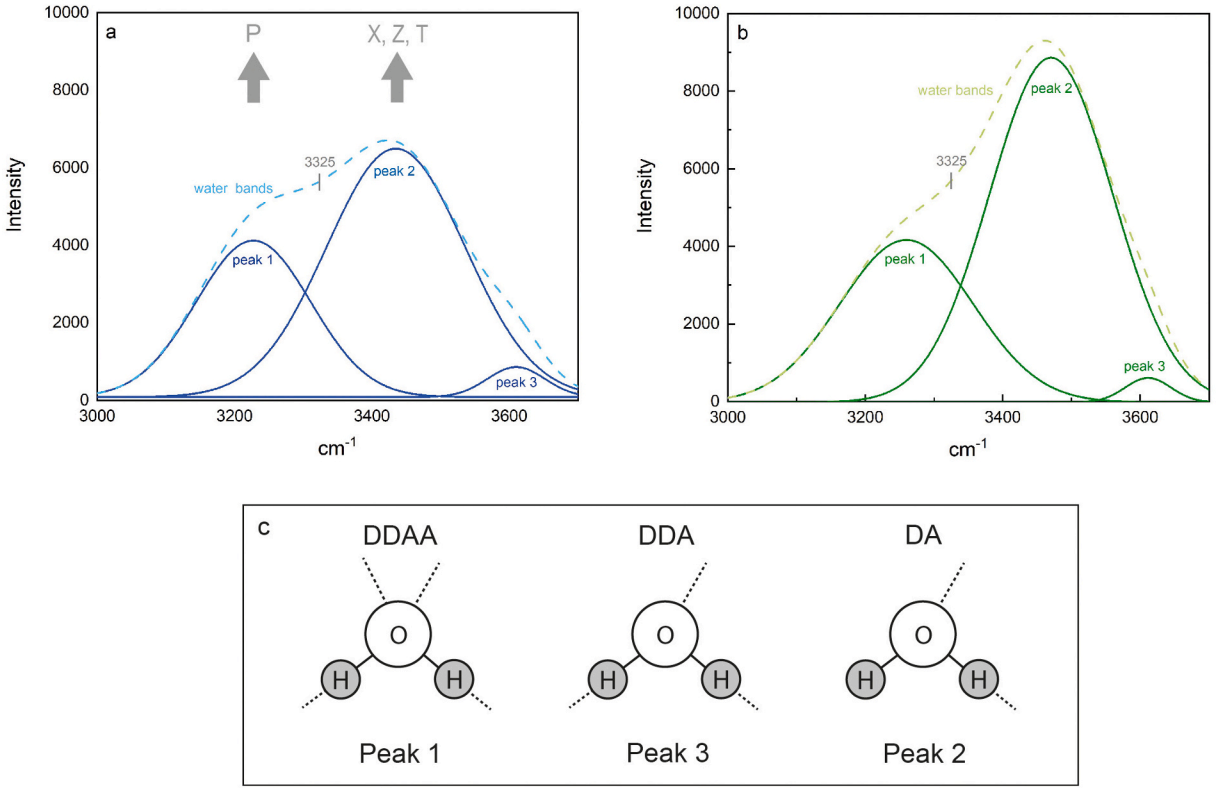

Fig. 4. The peak-deconvoluted Raman water bands are presented for a) pure water and b) 1.67 mol/l iodine, resolved into three Gaussian components. The resulting water bands are represented by dashed lines, with the inflection point of the water bands curve identified at 3325 cm^{-1}. Notably, with increasing iodine content (X) halogen ionic size (Z), and temperature (T), peak 2 becomes larger relative to peak 1, while pressure (P) has the opposing effect. In c), the components of the deconvolution are explained: Peak 1 is attributed to 4 hydrogen bonds per water molecule, involving two electron donors and two acceptors (DDAA). Peak 2 is attributed to 2 hydrogen bonds (DA). Peak 3 is attributed to 3 hydrogen bonds per water molecule (DDA) (Sun, 2009). The deconvolution of the Raman water bands confirms a reduction in hydrogen bonding in water with the addition of various halogens and their increasing ionic size. Moreover, increasing pressure correlates with an augmented number of hydrogen bonds.

$$S_D = \frac{\sum_{i=326}^{650}\left\{\frac{I(i)+I(i-1)}{2}*[n(i)-n(i-1)]\right\}}{\sum_{i=1}^{325}\left\{\frac{I(i)+I(i-1)}{2}*[n(i)-n(i-1)]\right\}}$$

Here, *n(i)* represents the shift at increment (or pixel) *i*, *I(i)* is the intensity at increment (or pixel) *i*, and the range of interest is between 3000 and 3650 cm^{-1} with a total of 650 pixels. This formula establishes the inflection point of the water bands at 3325 cm^{-1} (Fig. 4) and divides the water bands into two halves: left and right side from the inflection point. Đuričković et al. (2010) observed that S_D increases linearly with increasing NaCl concentration dissolved in water.

With increasing halogen concentration, the slope increases on both sides of the inflection point, resulting in an increase in both the sum of slopes for the left and right halves (cf., Fig. 2). This trend holds for all three studied halogens: chlorine, bromine, and iodine. To avoid division of two values that both correlate positively and increase with higher halogen concentrations, a ratio R_D was calculated, slightly different from S_D. The formula for R_D is as follows:

$$R_D = \frac{\sum_{i=1}^{325}\left\{\frac{I(i)+I(i-1)}{2}*[n(i)-n(i-1)]\right\}}{I_{i=1}*325}$$

Here again, *n(i)* represents the shift at increment (or pixel) *i*, *I(i)* is the intensity at increment (or pixel) *i*, and the total number of pixels considered is 325, starting from 3325 to 3650 cm^{-1}. This formula reduces some information loss from S_D and steepens the slope, as both the numerator and denominator of the ratio S_D increase with increasing halogen concentration.

However, the applicability of R_D is limited to liquid water. R_D does not account for strong changes in the shape of the slope, making it less suitable for high-pressure or low-temperature polymorphs (e.g., ice VI), which exhibit the dominant peak on the left side of the inflection point (Fig. 3).

4.3. Pressure

With increasing pressure, the water stretching band peak at 3428 cm^{-1} undergoes a reduction in intensity and shifts towards the left (e.g., Romanenko et al., 2018), while the smaller peak at 3240 cm^{-1} experiences a slight increase. The observed change stands in contrast to the effects observed during temperature increase (cf., Đuričković et al., 2010) or the addition of halogens (Fig. 3). This shift can be interpreted as a transition towards a higher number of hydrogen bonds (from DA to DDAA) in the water molecule network (Sun, 2009, Fig. 4). The effect is observable for all three halogens (chlorine, bromine, and iodine) in the saline solutions of this study (Fig. 3).

Sun (2012) did not observe the pressure effect in their chlorine data and argue against its existence. However, upon normalizing our data in the same way as Sun (2012), the peak at 3428 cm^{-1} decreases, and the water bands flatten, yet a clear pressure trend remains (Supplementary Fig. S1). It remains unclear why the trend was not observed in Sun (2012).

At pressures >1 GPa and ambient temperature, water transforms into ice VI (Fig. 3). Notably, with increasing halogen concentrations, the water-ice phase transformation shifts to higher pressures. In this study, liquid water/saline solution was observed at 1.1 GPa and 0.34 mol/l chlorine, 1.37 GPa and 0.97 mol/l bromine, or 1.27 GPa and 0.67 mol/l

iodine. The experimental setup does not precisely determine if the phase boundary shifts to higher pressure or if the liquid state is metastable. Journaux et al. (2013) investigated the impact of NaCl on the phase boundary of ice VI and found the boundary at 1.01 GPa for 1 mol/l, 1.09 GPa for 2.5 mol/l, and 1.52 GPa for 4 mol/l at ambient temperature. This boundary shift is much smaller than the observed range, suggesting a metastable liquid phase in our study or other kinetic effects.

As a consequence of the pressure-related shape change of the water stretching bands, R_D decreases with increasing pressure for fixed halogen concentrations (Fig. 3). Fig. 5 illustrates the R_D values vs. halogen concentration at different pressures (S_D values in Supplementary Fig. S2). Despite some outliers, the values follow a linear trend in the studied range, as previously observed for various temperatures (Đuričković et al., 2010). Within the range of comparable pressures, chlorine exhibits the lowest R_D values, while iodine demonstrates the highest. Comparable trends are also observed for integrated intensities (Supplementary Fig. S3) but show larger scatter relative to the R_D trends in Fig. 2d and Fig. 5.

4.4. Applications

4.4.1. Natural fluid inclusions with one unknown component (P or X)

R_D can be calculated from Raman spectra of natural fluid inclusions in minerals, as demonstrated by Kawamoto et al. (2013). In their study, saline fluid inclusions in spinel-harzburgite xenoliths collected from the 1991 Pinatubo pumice deposits were examined. The salinity of the fluid inclusions was reported as 5.1 ± 1 wt% NaCl equivalent (0.87 ± 0.17 mol/l), measured with microthermometry. The authors employed Raman spectroscopy for qualitative water measurements.

From the provided Raman spectrum, a R_D value of 0.79 can be calculated. The measured chlorine concentration from microthermometry allows for an estimate of the pressure to be around 0.5 GPa (Fig. 5a). This is notably lower than the 2–3 GPa that Kawamoto and colleagues estimated for the formation of the saline fluid inclusions in olivine below the Pinatubo. Given the available information, it can only be speculated whether some (parts) of the olivines formed at a very low pressure of 0.5 GPa, or if the inclusion lost pressure, and it was not fully closed above 0.5 GPa. In this case, the inclusion could at least partially represent the conditions at 0.5 GPa rather than at 2–3 GPa.

It is crucial to note that a fluid inclusion that closes between 810 °C and 1050 °C (Kawamoto et al., 2013) will experience a decrease in pressure when cooling down to ambient temperature. This phenomenon is also well observed in HDAC experiments (e.g., Bureau et al., 2010, 2016; Leroy et al., 2019; Louvel et al., 2020a, 2020b) and argues for a higher pressure than the 0.5 GPa that were obtained from the Raman spectrum. However, this sample serves as a good illustration of how pressure can be estimated by Raman in saline fluid inclusions with given salinity.

4.4.2. Natural fluid inclusions with two unknown components (P and X)

Difficulties arise when neither pressure nor salinity can be determined with a different method, and only the Raman spectrum is available. This scenario may occur for fluid inclusions that are too small for microthermometry, resulting in a single equation with two unknown parameters that cannot be solved for a distinct value.

Saline fluid inclusions from quartz samples analyzed by Pankrushina et al. (2020) illustrate the pressure dependence in Fig. 5d, where R_D values plot as a constant line. For instance, q1 has 1.9 mol/l NaCl at ambient pressure and 2.71 mol/l at 0.16 GPa; q2 has 1.88 mol/l and 2.69 mol/l; and q3 has 1.02 mol/l and 1.75 mol/l at ambient pressure and at 0.16 GPa, respectively. For an unknown pressure, a single salinity value cannot be determined this way. Particularly at lower salinity concentrations, the range of possible salinities can be drastic: for the three natural samples q1–3, a small pressure increase of 0.16 GPa changes the salinity by 42 to 72%. Given the stability field of quartz and saline fluids at room temperature, these are conservative calculations, and a much larger pressure range of >1 GPa must be considered.

However, fluid inclusions can be saturated in NaCl, and halite crystals do coexist with saline fluids in the inclusion (e.g., Brooks et al., 2019). The solubility of NaCl in water at ambient P-T conditions is 317 g/l or 5.4 mol/l (cf. Fig. 5). The pressure effect is diminished at NaCl-saturated conditions: Experiments in this study were conducted up to a salinity of 1.71 mol/l for NaCl, but assuming a continuation of the observed linear trend, the difference between 0 and 0.16 GPa would be only 16 to 18%.

Therefore, the pressure effect in fluid inclusions with high salinity is smaller than in fluid inclusions with low salinity. But as the potential pressure range is large (>1 GPa), ignoring the pressure effect can lead to a huge underestimation of the salinity in the fluid, and Raman spectroscopy alone cannot be used to determine reliable salinities in fluid inclusions.

4.4.3. Heavy halogens in HDAC experiments

The heavy halogens bromine and iodine typically play a minor role in natural fluid inclusions. The Cl/Br ratio in seawater is approximately 30, and the Cl/I ratio is around 50 (cf. Shaw and Cooper, 1957 for iodine). Due to enrichment and depletion processes in the Earth's mantle, Cl/Br ratios can vary significantly, ranging, for example, in diamond inclusions from 1 to 500 (Johnson et al., 2000). Despite their low concentration and minor role in fluid inclusions, heavy halogens are highly reactive and serve as important chemical agents in Earth's atmosphere (Fehn, 2012). Particularly for bromine, volcanoes have been recognized as significant contributors (Gerlach, 2004), if not the primary controlling factor (Pyle and Mather, 2009), to the current atmospheric content. This recognition is crucial, as bromine can be approximately 60 times more efficient (Sinnhuber et al., 2009) than chlorine in the destruction of stratospheric ozone (Daniel et al., 1999; Gerlach, 2004).

Over the past few decades, numerous studies have conducted high-pressure experiments on bromine- and iodine-bearing fluids interacting with silica melts in hydrothermal diamond anvil cells (HDAC). In these studies, the halogen content in the fluid was measured using synchrotron X-ray fluorescence (Bureau et al., 2010, 2016; Grützner et al., 2024; Kawamoto et al., 2014; Leroy et al., 2019; Louvel et al., 2020a, 2020b). These experiments provide valuable insights into the behavior of heavy halogens during fluid-magma degassing processes.

However, these experiments entail complex setups and lack reliable and easily adaptable pressure sensors. The fluorescence wavelength shift of ruby is a commonly used pressure sensor (e.g., Chervin et al., 2001; Shen et al., 2020), but it cannot be applied in experiments conducted at elevated temperatures where ruby spheres dissolve. Other pressure indicators, like X-ray diffraction of gold particles, are only reliable at higher temperatures (cf. Grützner et al., 2024; Louvel et al., 2020b). Pressure monitoring in these HDAC experiments is essential to understand the pressure effect on halogen partitioning between silicate melts and aqueous fluids. Moreover, it is crucial to exclude pressure loss processes during the experiment (cf. Bureau et al., 2010, 2016; Leroy et al., 2019; Louvel et al., 2020a, 2020b).

Most HDAC experiments are conducted at high temperatures, reaching several hundred degrees Celsius (e.g., Bureau et al., 2010, 2016; Grützner et al., 2024; Leroy et al., 2019; Louvel et al., 2020a, 2020b). The elevated temperature introduces an additional variable to the shift change of the water bands, as they also change with varying temperature (Krishnamurthy et al., 1983; Ratcliffe and Irish, 1982).

Thus far, residual pressure can be monitored at ambient temperature, for example, before and after the experiment, once the fluid has been cooled down to room temperature. Fig. 5e illustrates two samples used for test measurements, following the experimental setup and the analytical methods for bromine concentration reported in Grützner et al. (2024). These samples represent experiments that tested the degassing reaction of a bromine-doped basalt melt into an aqueous fluid. Experiments were conducted at high temperatures (above the basalt solidus) and pressures of up to 1.7 GPa in a HDAC (cf. Grützner et al., 2024, for a

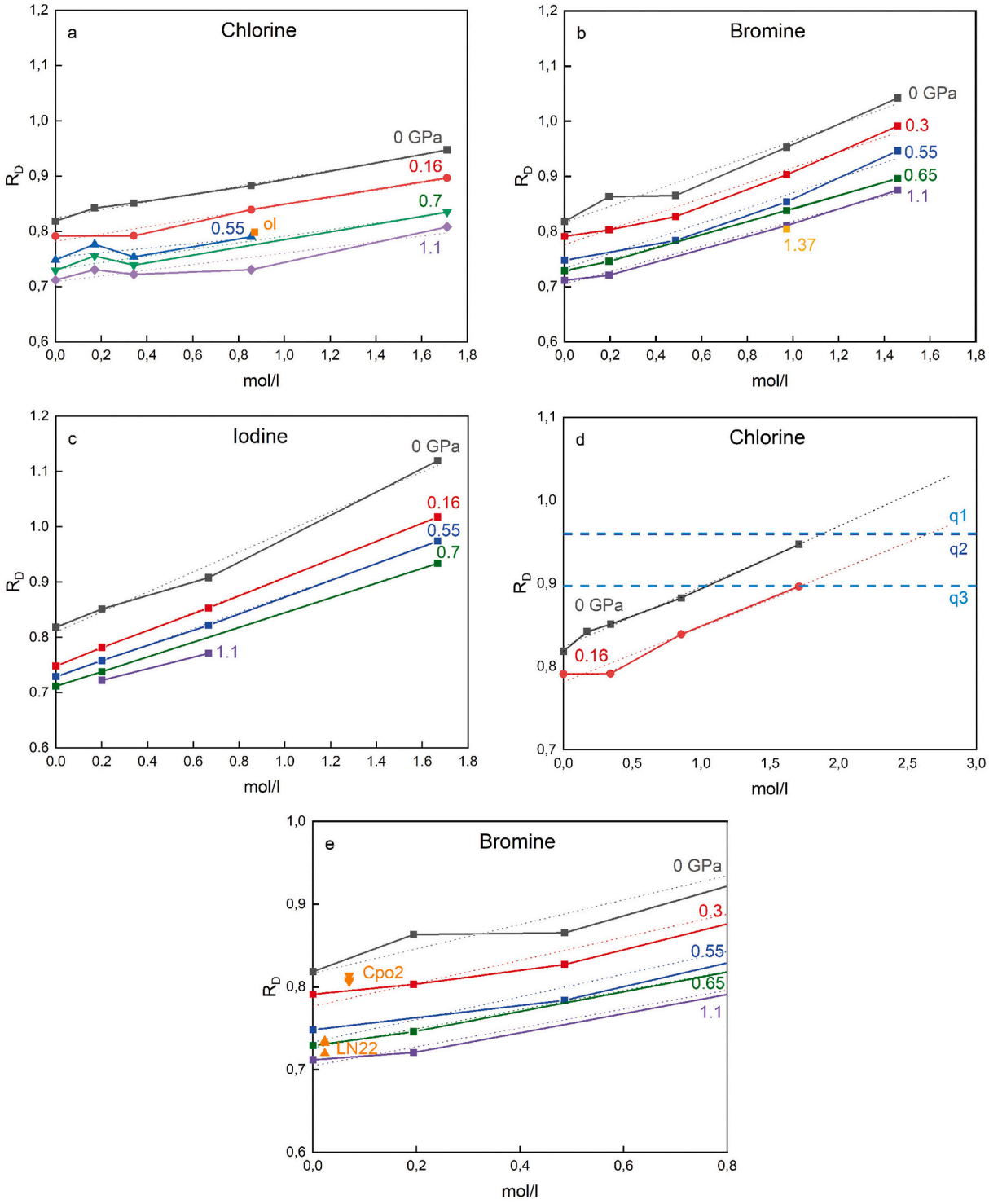

Fig. 5. R_D values vs halogen concentration for (a) chlorine, (b) bromine, and (c) iodine are presented in the figure. The colored lines indicate isobars: the solid lines connect the data points, while the dashed lines represent trend lines. Like the Raman water bands and the R_D values, the isobars exhibit the steepest slope for high concentrations of iodine and become flatter with smaller ionic halogen size, but also with increasing pressure. (a) "ol" data are from a natural fluid inclusion in olivine (Kawamoto et al., 2013). (d) Calculated R_D values for natural fluid inclusions in quartz demonstrate the pressure effect: q1 has 1.9 mol/l NaCl equivalent at ambient pressure and 2.71 mol/l at 0.16 GPa; q2 has 1.88 mol/l and 2.69 mol/l; and q3 has 1.02 mol/l and 1.75 mol/l at ambient pressure and at 0.16 GPa, respectively. The fluid inclusions were analyzed by Pankrushina et al. (2020) (sample names are q1 = 672; q2 = 33,604; q3 = 20,512). (e) Cpo2 and LN22 are experimental HDAC samples. Bromine content was analyzed with X-ray fluorescence following the methods reported in Bureau et al. (2010) and Grützner et al. (2024).

detailed description of the experiments). Bromine concentrations of 0.07 mol/l for sample LN22 and 0.023 mol/l for Cpo2 were measured in the fluid by synchrotron x-ray fluorescence (SXRF) during the experiments. Raman spectra of the aqueous fluids were analyzed after the experiment under room temperature conditions. Bromine concentrations from SXRF, together with the Raman spectra, allow estimating pressure ranges of 0.7 to 0.9 GPa for LN22 and 0.1 to 0.2 GPa for Cpo2. These promising results show that Raman water bands can be used as pressure or salinity indicators from room to high temperatures, providing additional pressure-concentration-related temperature calibrations are performed.

5. Conclusion

Our new experimental dataset demonstrates that the impact of halogens on the change of Raman water band shifts increases with ionic size from chlorine over bromine to iodine. To address and compare these changes, we calculated the numerical value R_D. Our experiments further show that increased pressure diminishes the impact of the halogen shift change to a different extent for each of the three halogens. This can have drastic consequences for the salinity calculation of fluid inclusions in minerals like quartz or olivine. Especially in the range of low salinity, the concentration can be strongly underestimated if the pressure effect is ignored. Either pressure or salinity needs to be determined by an independent method. For experiments performed in diamond anvil cells with halogens in aqueous fluids, the change of Raman water band shifts can be a beneficial (with some restrictions) tool to monitor the pressure at room temperature, if salinity is known, and inversely this change can be used to monitor the salinity.

Supplementary data to this article can be found online at https://doi.org/10.1016/j.chemgeo.2024.122065.

Statement

During the preparation of this work the authors used ChatGPT 3.5 to correct errors of spelling, punctuation, grammar and to improve the syntax in several chapters of the manuscript. After using this tool, the authors reviewed and edited the content and take full responsibility for the content of the publication.

CRediT authorship contribution statement

Tobias Grützner: Writing – review & editing, Writing – original draft, Visualization, Validation, Software, Resources, Project administration, Methodology, Investigation, Formal analysis, Data curation, Conceptualization. **Hélène Bureau:** Writing – review & editing, Validation, Supervision, Resources, Project administration, Methodology, Funding acquisition, Conceptualization.

Declaration of competing interest

Tobias Grützner reports financial support was provided by European Commission. Hélène Bureau reports financial support was provided by French National Research Agency. If there are other authors, they declare that they have no known competing financial interests or personal relationships that could have appeared to influence the work reported in this paper.

Data availability

I have shared the link to my data at the Attach File step.

Raman Water bands on experimental sodium-halogen solutions at various pressure and concentration (Original data) (Mendeley Data)

Acknowledgments

This project was funded by the ANR Projet de Recherche Collaborative VOLC-HAL-CLIM (Volcanic Halogens: from Deep Earth to Atmospheric Impacts), ANR-18-CE01-0018 (Hélène Bureau). Tobias Grützner is grateful for the EU Marie Skłodowska-Curie Fellowship "ExCliso" (Project ID 101017762). We thank K. Béneut for his support with the Raman laser we used for our experiments at the IMPMC and Y. Guarnelli for his help with the DAC alignment. We are very grateful to E.A. Pankrushina for providing the raw dataset of Raman spectra from her study. We thank the two reviewers for their helpful comments to improve the manuscript and Claudia Romano is warmly thanked for handling the manuscript.

References

Aiuppa, A., Baker, D.R., Webster, J.D., 2009. Halogens in volcanic systems. Chem. Geol. 263 (1–4), 1–18. https://doi.org/10.1016/j.chemgeo.2008.10.005.

Bakker, R.J., 2004. Raman spectra of fluid and crystal mixtures in the systems H_2O, H_2O-NaCl and H_2O-$MgCl_2$ at low temperatures: applications to fluid-inclusion research. Can. Mineral. 42, 1283–1314. https://doi.org/10.2113/gscanmin.42.5.1283.

Besemer, M., Bloemenkamp, R., Ariese, F., van Manen, H.-J., 2016. Identification of multiple water−iodide species in concentrated NaI solutions based on the raman bending vibration of water. J. Phys. Chem. A 120 (5), 709–714. https://doi.org/10.1021/acs.jpca.5b10102.

Brooks, H.L., Dragovic, B., Lamadrid, H.M., Caddick, M.J., Bodnar, R.J., 2019. Fluid capture during exhumation of subducted lithologies: a fluid inclusion study from Sifnos, Greece. Lithos 332-333, 120–134. https://doi.org/10.1016/j.lithos.2019.01.014.

Bureau, H., Foy, E., Raepsaet, C., Somogyi, A., Munsch, P., Simon, G., Kubsky, S., 2010. Bromine cycle in subduction zones through in situ Br monitoring in diamond anvil cells. Geochim. Cosmochim. Acta 74, 3839–3850. https://doi.org/10.1016/j.gca.2010.04.001.

Bureau, H., Auzende, A.-L., Marocchi, M., Raepsaet, C., Munsch, P., Testemale, D., Mézouar, M., Kubsky, S., Carrière, M., Ricolleau, A., Fiquet, G., 2016. Modern and past volcanic degassing of Iodine. Geochim. Cosmochim. Acta 173, 114–125. https://doi.org/10.1016/j.gca.2015.10.017.

Chervin, J.C., Canny, B., Mancinelli, M., 2001. Ruby-spheres as pressure gauge for optically transparent high pressure cells. High Press. Res. 21, 305–314. https://doi.org/10.1080/08957950108202589.

Daniel, J.S., Solomon, S., Portmann, R.W., 1999. Stratospheric ozone destruction: the importance of bromine relative to chlorine. J. Geophys. Res. 104, 23871–23880. https://doi.org/10.1029/1999JD900381.

Dubessy, J., Lhomme, T., Boiron, M.-C., Rull, F., 2002. Determination of chlorinity in aqueous fluids using Raman spectroscopy of the stretching band of water at room temperature: application to fluid inclusions. Appl. Spectrosc. 56 (1), 99–106.

Đuričković, I., Marchetti, M., Claverie, R., Bourson, P., Chassot, J.-M., Fontana, M.D., 2010. Experimental study of NaCl aqueous solutions by Raman spectroscopy: Towards a new optical sensor. Appl. Spectrosc. 64 (8), 853–857. https://doi.org/10.1366/000370210792080984.

Fehn, U., 2012. Tracing crustal fluids: applications of natural 129I and 36C. Annu. Rev. Earth Planet. Sci. 40, 45–67. https://doi.org/10.1146/annurev-earth-042711-105528.

Georgiev, G.M., Kalkanjiev, T.K., Petrov, V.P., Nickolov, Zh., 1984. Determination of Salts in Water Solutions by a Skewing Parameter of the Water Raman Band. Appl. Spectrosc. 38 (4), 593–595. https://doi.org/10.1366/0003702844555106.

Gerlach, T.M., 2004. Volcanic source of tropospheric ozone-depleting trace gases. Geochem. Geophys. Geosyst. 5, Q09007. https://doi.org/10.1029/2004GC000747.

Grützner, T., Bureau, H., Boulard, E., Munsch, P., Guignot, N., Siebert, J., Guarnelli, Y., 2024. An in-situ experimental HP/HT study on bromine release from a natural basalt. Chem. Geol. 644, 121869 https://doi.org/10.1016/j.chemgeo.2023.121869.

Johnson, L.H., Burgess, R., Turner, G., Milledge, H.J., Harris, J.W., 2000. Noble gas and halogen geochemistry of mantle fluids: comparison of African and Canadian diamonds. Geochim. Cosmochim. Acta 64, 717–732. https://doi.org/10.1016/S0016-7037(99)00336-1.

Journaux, B., Daniel, I., Caracas, R., Montagnac, G., Cardon, H., 2013. Influence of NaCl on ice VI and ice VII melting curves up to 6 GPa, implications for large icy moons. Icarus 226, 355–363. https://doi.org/10.1016/j.icarus.2013.05.039.

Kawamoto, T., Yoshikawa, M., Kumagai, Y., Mirabueno, M.H.T., Okuno, M., Kobayashi, T., 2013. Mantle wedge infiltrated with saline fluids from dehydration and decarbonation of subducting slab. Proc. Natl. Acad. Sci. U. S. A. 110 (24), 9663–9668. https://doi.org/10.1073/pnas.1302040110.

Kawamoto, T., Mibe, K., Bureau, H., Reguer, S., Mocuta, C., Kubsky, S., Thiaudière, D., Ono, S., Kogiso, T., 2014. Large-ion lithophile elements delivered by saline fluids to the sub-arc mantle. Earth Planets Space 66, 61. https://doi.org/10.1186/1880-5981-66-61.

Krishnamurthy, S., Bansil, R., Wiafe-Akente, J., 1983. Low-frequency Raman spectrum of supercooled water. J. Chem. Phys. 79, 5863–5870. https://doi.org/10.1063/1.445756.

Leroy, C., Bureau, H., Sanloup, C., Raepsaet, C., Glazirin, K., Munsch, P., Harmand, M., Prouteau, G., Khodja, H., 2019. Xenon and iodine behaviour in magmas. Earth Planet. Sci. Lett. 522, 144–154. https://doi.org/10.1016/j.epsl.2019.06.031.

Louvel, M., Cadoux, A., Brooker, R.A., Proux, O., Hazemann, J.-L., 2020a. New insights on Br speciation in volcanic glasses and structural controls on halogen degassing. Am. Min. 105, 795–802. https://doi.org/10.2138/am-2020-7273.

Louvel, M., Sanchez-Valle, C., Malfait, W.J., Pokrovski, G.S., Borca, C.N., Grolimund, D., 2020b. Bromine speciation and partitioning in slab-derived aqueous fluids and silicate melts and implications for halogen transfer in subduction zones. Solid Earth 11, 1145–1161. https://doi.org/10.5194/se-11-1145-2020.

Mernagh, T.P., Wilde, A.R., 1989. The use of the laser Raman microprobe for the determination of salinity in fluid inclusions. Geochim. Cosmochim. Acta 53 (4), 765–771. https://doi.org/10.1016/0016-7037(89)90022-7.

Moncada, D., Bodnar, R.J., 2012. Raman spectroscopy technique to determine the salinity of fluid inclusions, PACROFI-XI (Pan-American Current Research on Fluid Inclusions) Conference, p. 67.

Ni, P., Ding, J., Rao, B., 2006. In situ cryogenic Raman spectroscopic studies on the synthetic fluid inclusions in the systems H_2O and NaCl-H_2O. Chin. Sci. Bull. 51 (1), 108–114. https://doi.org/10.1007/s11434-004-0256-5.

Pankrushina, E.A., Krupenin, M.T., Shchapova, Y.V., Kobuzov, A.S., Garaeva, A.A., Votyakov, S.L., 2020. The study of fluid inclusion salinity in minerals by raman spectroscopy revisited. In: Votykov, S., Kiseleva, D., Grokhovsky, V., Shchapova, J. (Eds.), Minerals: Structure, Properties, Methods of Investigation: Proceedings of the 10th all-Russian Youth Scientific Conference (pp. 175–183). Springer International Publishing. https://doi.org/10.1007/978-3-030-49468-1_23.

Pyle, D.M., Mather, T.A., 2009. Halogens in igneous processes and their fluxes to the atmosphere and oceans from volcanic activity: a review. Chem. Geol. 263, 110–121. https://doi.org/10.1016/j.chemgeo.2008.11.013.

Ratcliffe, C.I., Irish, D.E., 1982. Vibrational spectral studies at elevated temperatures and pressures. Raman studies of liquid water up to 300 °C. J. Phys. Chem. 86, 4897–4905. https://doi.org/10.1021/j100222a013.

Romanenko, A.V., Rashchenko, S.V., Goryainov, S.V., Likhacheva, A.Y., Korsakov, A.V., 2018. In situ Raman study of liquid water at high pressure. Appl. Spectrosc. 72 (6), 847–852. https://doi.org/10.1177/0003702817752487.

Shaw, T., Cooper, L., 1957. State of Iodine in Sea Water. Nature 180, 250. https://doi.org/10.1038/180250a0.

Shen, G., Wang, Y., Dewaele, A., Wu, C., Fratanduono, D.E., Eggert, J., Klotz, S., Dziubek, K.F., Loubeyre, P., Fat'yanov, O.V., Asimov, P.D., Mashimo, T., Wentzcovitch, R.M.M., 2020. Toward an international practical pressure scale: a proposal for an IPPS ruby gauge (IPPS-Ruby2020). High Press. Res. 40 (3), 299–314. https://doi.org/10.1080/08957959.2020.1791107.

Sinnhuber, B.-M., Sheode, N., Sinnhuber, M., Chipperfield, M.P., Feng, W., 2009. The contribution of anthropogenic bromine emissions to past stratospheric ozone trends: a modelling study. Atmos. Chem. Phys. 9 (8), 2863–2871. https://doi.org/10.5194/acp-9-2863-2009.

Sun, Q., 2009. The Raman OH stretching bands of liquid water. Vib. Spectrosc. 51, 213–217. https://doi.org/10.1016/j.vibspec.2009.05.002.

Sun, Q., 2012. Raman spectroscopic study of the effects of dissolved NaCl on water structure. Vib. Spectrosc. 62, 110–114. https://doi.org/10.1016/j.vibspec.2012.05.007.

Sun, Q., Zhao, L., Li, N., Liu, J., 2010. Raman spectroscopic study for the determination of Cl-concentration (molarity scale) in aqueous solutions: Application to fluid inclusions. Chem. Geol. 272 (1–4), 55–61. https://doi.org/10.1016/j.chemgeo.2010.02.004.

Terpstra, P., Combes, D., Zwick, A., 1990. Effect of salts on dynamics of water: a Raman spectroscopy study. J. Chem. Phys. 92, 65–70. https://doi.org/10.1063/1.458418.

Walrafen, G.E., Fisher, M.R., Hokmabadi, M.S., Yang, W.-H., 1986. Temperature dependence of the low- and high-frequency Raman scattering from liquid water. J. Chem. Phys. 85 (12), 6970–6982. https://doi.org/10.1063/1.451384.